

1 Stratification and Mixed Layer Depth around 2 Iceland: Characterization and inter-annual 3 variability

4 Angel Ruiz-Angulo ^{1*}, Esther Portela ², Charly de Marez¹, Andreas Macrander³,
5 Sólveig Rósa Ólafsdóttir³, Thomas Meunier ⁴, Steingrímur Jónsson ^{3,5}, and M. Dolores
6 Pérez-Hernández ⁶

7 ¹Earth Science Institute, University of Iceland, 101 Reykjavik, Iceland

8 ²Univ. Brest, Laboratoire d'Océanographie Physique et Spatiale, CNRS, IRD, Ifremer, Plouzané, France

9 ³Hafrannsóknastofnun / Marine and Freshwater Research Institute, Hafnarfjörður, Iceland,

10 ⁴Woods Hole Oceanographic Institution, Woods Hole MA, USA

11 ⁵University of Akureyri, Akureyri, Iceland

12 ⁶Unidad océano y clima, Instituto de Oceanografía y Cambio Global, IOCAG, Universidad de Las Palmas de Gran Canaria,
13 ULPGC, Unidad Asociada ULPGC-CSIC, Las Palmas de Gran Canaria, Spain

14 *Correspondence to:* Angel Ruiz-Angulo (angel@hi.is)

15 ABSTRACT

16 The ocean around Iceland is a key region where major water masses and currents interact, influencing the global ocean
17 circulation. Here, we analyze 29 years (1990-2019) of quarterly hydrographic section data collected around Iceland. The
18 hydrographic properties around Iceland show important spatial variability. Based on temperature, salinity, and stratification
19 structure, we classified the Icelandic waters in three distinct regions: the south, the north, and northeast regions. The warm
20 and salty Atlantic Waters that dominate the south show the deepest winter mixed layers (~500m) while the north and
21 northeast show shallower depths (~100m). Based on the decomposition of total stratification into temperature and salinity
22 contributions, we find that the subsurface stratification is mainly controlled by temperature in the south and by salinity in
23 the northwest, while in the north, the North Icelandic Irminger Current and East Icelandic Current alternate seasonally,
24 shifting the region between temperature-dominated and salinity-dominated stratification. The interannual variability of the
25 mixed layer and of its thermohaline properties is also large around Iceland. Mixed layer waters were generally colder in
26 the 90's, then warmed until approximately 2015, and became colder again from 2015 to 2018. In the northeast, a
27 multidecadal mixed layer warming trend emerges from the interannual variability as the Atlantic Water progresses
28 northeastward, which is responsible for transforming locally the upper stratification from salinity-dominated into
29 temperature-dominated. This is associated with the “Atlantification” of the Arctic. Within the mixed layer south of Iceland,
30 density has continuously decreased since the mid 1990's. Elsewhere, we observe density-compensated changes in mixed
31 layer temperature and salinity, without clear long trends. This study provides an unprecedented and detailed description of
32 the seasonal to multi-decadal variability of the mixed layer depth and stratification around Iceland, showing links between
33 this regional variability and changing North Atlantic under global warming.

34 **Keywords:** Mixed layer depth, Mixed layer properties, stratification, Ocean warming, Atlantification, Interannual
35 variability

36

37 1 INTRODUCTION

38 The ocean around Iceland is a key region where major water masses and currents interact, shaping the North Atlantic
39 circulation, and play a crucial role on the Atlantic Meridional Overturning Circulation (AMOC). The Nordic Seas are
40 among the few places on the globe where the formation of deep waters (1000-3000 m depth) occurs during winter deep
41 convection (Petit et al., 2020). The southern end of the Nordic Seas is bounded by the Greenland-Iceland-Scotland Ridge
42 (GISR). The North Atlantic Current (NAC) brings the warm and salty Atlantic Water (AW) northward into the Nordic Seas
43 (Hátún and Chafik, 2018; Østerhus et al., 2019; Hátún et al., 2021). The AW crosses the ridge in three ways (Fig. 1): (i)
44 between Greenland and Iceland, where the Irminger Current (IC) forms the North Icelandic Irminger Current (NIIC)
45 bringing AW that flows clockwise around Iceland (Jónsson & Briem, 2003; Jónsson & Valdimarsson, 2012); (ii) between
46 Iceland and the Faroe Islands (Mauritzen, 1996); and (iii) through the Faroe Shetland Channel (Hansen and Østerhus, 2000;
47 Hansen et al., 2023), contributing up to 48% of the total AW transport. The AW undergoes strong cooling and densification
48 in the Nordic Seas and the Arctic Ocean (Mauritzen, 1996; Pérez-Hernández et al., 2019; Athanase et al., 2020; Huang et
49 al., 2023). This modified AW is referred to as Atlantic-origin Overflow Water (AtOW; *e.g.*, Havik et al., 2017; Casanova-
50 Masjoan et al., 2020) and is one of the two sources of Denmark Strait Overflow Water (DSOW; Semper et al. 2019). AtOW
51 travels southward as a mid-depth water mass in the East Greenland Current (EGC; Håvik et al., 2017), from where, part of
52 it diverts east and merges with the NIIC northeast of Iceland (Casanova-Masjoan et al., 2020).

53 The transformation of AW into AtOW takes place in different areas of the Nordic Seas: along the Norwegian Current
54 (Håvik et al., 2017), in the Iceland Sea Gyre (Våge et al., 2013), on the eastern side of Greenland, or even –due to its
55 proximity– in the Arctic Basin (Pérez-Hernández et al., 2019). This transformation has different driving mechanisms
56 impacting mixing and convective processes. Wind-stress, sea-ice retreat, and high heat loss due to cold-air outbreaks drive
57 the transformation east of Greenland (Våge et al., 2018). Sea-ice retreat, and heat exchange dominate north of Svalbard
58 (Pérez-Hernández et al., 2019; Athanase et al., 2020), and heat fluxes are the main drivers in the center of Iceland Sea
59 (Våge et al., 2013). Thus, the Nordic Seas region has been previously described as a “mixing pot” (Renfrew et al., 2019),
60 largely responsible for the overall formation of deep overflow water (Lozier et al., 2019). The Nordic Seas are also a large
61 repository of freshwater, primarily originated from glacier melt and river discharge. This water mass increases buoyancy
62 and is carried southward by the East Greenland Current (EGC). Therefore, it is crucial to fully understand the variability
63 of the upper ocean, where mixed layers (ML) develop and transform these water masses.

64 The Arctic Ocean is warming much faster than the global average, a process known as “Arctic Amplification,” which is
65 also associated with the “Atlantification” of the Arctic (Polyakov et al., 2017; Dai et al., 2019). While the causes are still
66 debated, Arctic Amplification has evident consequences, such as a decrease in seasonal sea-ice extent and a weakening of
67 the cold halocline (Polyakov et al., 2020; Dai et al., 2019). Although these changes are less pronounced in the central
68 Iceland Sea, similar processes have been observed in the central Greenland Sea and the northeastern shelf (Gjelstrup et al.,
69 2022; Strehl et al., 2024), suggesting that Atlantification may also influence the Iceland Sea. Changes in temperature and
70 salinity in the upper ocean modify upper-ocean stratification, which partially controls the mixed layer depth (MLD).

71 The depth and structure of the ML is primarily controlled by local buoyancy forcing, *i.e.*, surface heat loss and freshwater
72 fluxes, which modifies the water density (Kohler et al., 2018). For instance, within the Iceland Basin, wintertime buoyancy
73 loss drives deep convection, shaping the thermohaline properties that influence the lower limb of the AMOC and its
74 variability in the subpolar North Atlantic (Petit et al., 2021). The pre-existing stratification of the water column is
75 responsible for controlling the effect of the surface forcing. Strongly stratified upper layers resist mixing, while weak
76 stratification allows deeper penetration of turbulence and convection mixing (Pierce et al., 1986). Over shorter timescales,
77 on the order of days, the MLD can significantly deepen as a result of the strong wind events with significant wind stress

78 and associated large wave heights (Skylingstad et al., 2023). MLD and stratification are strongly influenced by
79 atmospheric forcing, including variability associated with the North Atlantic Oscillation (NAO), which modulates wind
80 stress, surface heat flux, and freshwater input in the Iceland region (Hurrell, 1995; Dickson et al., 1996)

81 The Intergovernmental Panel on Climate Change (IPCC), Special Report on the Ocean and Cryosphere in a Changing
82 Climate (IPCC-SROCC 2019), indicates with *high confidence* that roughly 40% of the global ocean mean upper ocean
83 stratification has increased about 3.3–6.1% since 1960 due to both oceans warming and high-latitude freshening (Tesdal et
84 al., 2018; Yamaguchi and Suga, 2019; Bindoff et al., 2019; Liu et al., 2020; Sallée et al., 2021). Increased stratification is
85 associated with less efficient diapycnal mixing, reducing the exchanges of heat and tracers from the mixed layer into the
86 ocean interior. It has also been observed, with *high confidence*, that the ML is undergoing changes (Bindoff et al., 2019;
87 on Climate Change, IPCC). Particularly, the shallow summertime ML, which is more likely to be affected by global
88 warming, is deepening at a rate of 5 – 10 m per decade (Sallée et al., 2021). Despite the reported global patterns, it has
89 been also acknowledged that regional changes might differ from the global estimates (Fox-Kemper et al., 2021).

90 The warming of the ML and the associated increase in stratification have an impact in biogeochemical processes like
91 phytoplankton blooms and carbon or oxygen sequestration, key components for the Earth’s climate (Olafsson, 2003; Pérez
92 et al., 2021). In the waters surrounding Iceland, the phytoplankton community is closely linked with the water mass
93 properties and hence, an “Atlantification” will replace Polar communities with more Atlantic communities (Cerfonteyn et
94 al. 2023). In the Arctic Ocean, north and northwest of Iceland, the early onset of stratification in spring gives rise to rapid
95 shallowing of the mixed layer and triggers early spring phytoplankton blooms, whereas the weakly stratified water-column
96 in the Atlantic water and the associated deep ML delay the spring bloom south of Iceland (Zhai et al., 2012). This also has
97 strong consequences in carbon uptake, vertical nutrient supply, and biological processes (Yamaguchi and Suga, 2019).
98 Other indirect impacts of the increased stratification include changes in upwelling, deep-water formation rates, biological
99 production, and remineralization rates (Holt et al., 2016), and deoxygenation (Shepherd et al., 2017).

100 Thus, the overall goal of this study is to characterize the spatial and temporal variability of the mixed layer and
101 stratification around Iceland, where Atlantic Water inflow, Arctic waters, and local surface fluxes shape upper-ocean
102 properties. Using a 29-year hydrographic time series, we investigate the variability of water-mass properties, mixed-layer
103 depth (MLD), density, and thermohaline structure across seasonal and interannual timescales. We examine correlations
104 with atmospheric circulation patterns such as the North Atlantic Oscillation (NAO) and, to complement the observations,
105 use a 1D PWP model to simulate the mixed-layer response to local forcing, helping to identify the mechanisms driving
106 MLD variability.

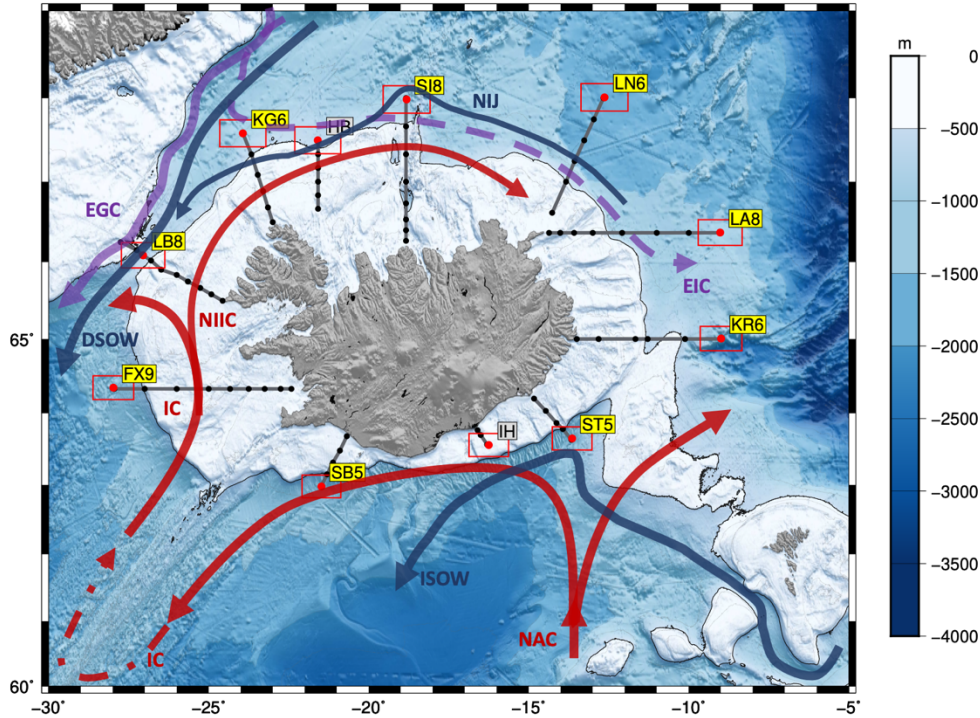
107 2 DATA AND METHODS

108

109 We use Conductivity-Temperature-Depth (CTD) data from the repeated hydrographic observational program of the
110 Icelandic Marine and Freshwater Research Institute between 1990 and 2019. The oceanographic surveys took place
111 quarterly, mainly in February, May, August, and November with little coverage during the intermediate months.
112 Observations are made at standard repeated sections. The profiles are obtained with a Seabird 911plus CTD mounted on a
113 rosette with Niskin bottles. The conductivity data are calibrated with salinity samples taken at the bottom of each station.
114 All sensors underwent regular calibrations by the manufacturer.

115 In our analyses we considered only the deepest stations in each section (red dots in Fig. 1), including nearby stations
116 within an area defined by $1^\circ \times 0.5^\circ$ in longitude and latitude (red boxes). The selected stations are located outside of the

117 Icelandic shelf (about 500 m depth). This criterion was chosen to avoid topographic effects, such as across shelf processes
 118 on the stratification of the water column and to avoid MLDs limited by shallow bathymetry. Thus, the stations in gray, HB
 119 and IH in Figure 1 were not considered as they fall on the shelf. For the sake of simplicity stations will be named with the
 120 acronym of the standard section, first two letters and the station number. The station full name (section and station number)
 121 can be found in Table 1.



122
 123 **Figure 1: Map of the typical hydrographic sections collected by the Marine and Freshwater Research Institute around Iceland; the**
 124 **black dots represent the nominal location of the standard stations from 1990-2019. The red dots are the stations used for this analysis**
 125 **and the red boxes delimit the area within which all data were considered for this study. The grey bathymetric contours are spaced**
 126 **every 100 m for the shallow water until the 500 m depth (thick black line) and then every 500 m. The hydrographic stations shown**
 127 **in the yellow boxes corresponding to the standard sections: Faxaflói (FX9), Látrabjarg (LB8), Kögur (KG6), Hornbanki (HB),**
 128 **Siglunes (SI8), Langanes NE (LN6), Langanes E (LA8), Krossanes (KR6), Stokksnes (ST5), Ingólfshöfði (IH) and Selvogsbanki**
 129 **(SB5). The gray labeled IH and HB were not used in this analysis. The main surface and deep currents are also depicted on the map.**

130 In this study we analyze the inter-annual variability and linear trends of the ML over a 29-year period as well as the
 131 seasonal variability using the seasonal extremes (summer and winter), when there is more data coverage. From the CTD
 132 stations we estimated the MLD using the density threshold method with a criterion of $\sigma_\theta = 0.01 \text{ kg m}^{-3}$ (as, for instance,
 133 in Piron et al., (2016) in the Irminger Sea) and a reference depth of 10 m. We chose this criterion instead of the usual 0.03
 134 kg m^{-3} (de Boyer Montégut, 2004) as the latter overestimated the MLD in more than 500 visually inspected profiles (not
 135 shown). For comparison and robustness of our chosen method, we also estimated the MLD using other criteria (de Boyer
 136 Montégut et al., 2004; Holte et al., 2017). We found the density threshold method appropriate for our region as it proves to
 137 be effective even for cases where the variations of salinity and temperature were large. Those variations usually compensate
 138 in density making this method more suitable. We have validated our method against previous work by Våge et al., (2018),
 139 where a glider data were available, and the results were satisfactory. However, automatic detection methods have
 140 limitations, as they may miss stacked mixed layers and other non-canonical representation MLDs.

141 For each profile we computed the Brunt -Väisälä frequency (N^2), defined as:

142
$$N^2 = g \frac{1}{\rho_0} \frac{\partial \sigma_\theta}{\partial z}, \quad (1)$$

143 where g is the acceleration due to gravity, ρ_0 is a reference density, σ_θ is the potential density and z is depth. N^2 can be
144 decomposed to show the relative contribution of salinity and temperature to the observed stratification as follows:

145
146
$$N^2 = N_T^2 + N_S^2, \quad (2)$$

147 where N_T^2 and N_S^2 are the components representing the stratification set by the temperature and salinity, respectively and
148 are defined as:

149
$$N_T^2 = g \left(\alpha \frac{\partial T}{\partial z} \right), \quad (3)$$

150
151
$$N_S^2 = g \left(\beta \frac{\partial S}{\partial z} \right), \quad (4)$$

152 where α is the thermal expansion coefficient and β is the haline contraction coefficient at constant pressure. This
153 decomposition has also been made to classify the oceans by their stratification contribution into α -ocean, β -ocean, and
154 transition zone, where in α -oceans stratification is permanently dominated by temperature, in β -oceans by salinity and the
155 transition regions are either intermittently or seasonally dominated by temperature or salinity (Carmack, 2007; Stewart and
156 Haine, 2016). For the water column to be statically stable, N^2 must be positive. However, the contributions may not be
157 positive; when either of its components, N_T^2 or N_S^2 are negative, temperature or salinity respectively has a destabilizing
158 effect on the resulting stratification that must be compensated by the other variable to maintain a stable water column. Small
159 values of N^2 indicate that the water column is weakly stratified, which favors mixing due to winter convection and deeper
160 MLD.

161 To investigate further the driving mechanism of the MLD, we used the Price-Weller-Pinkel (PWP) model (Pierce et al.,
162 1986). The PWP model was chosen to test the hypothesis that β - and transition oceans do not develop deep mixed layers,
163 which is shown in Figure 8. The PWP model is a one-dimensional vertical model used to simulate the evolution of the
164 ocean mixed layer in response to atmospheric forcing, including wind stress, heat fluxes, and freshwater fluxes. The
165 model evolves vertical profiles of temperature, salinity, density, and horizontal velocity based on surface forcing and a set
166 of physical stability criteria. The first criterion is convective overturning. If surface cooling increases the density such that
167 the water column becomes gravitationally unstable (i.e., denser water overlies lighter water), the model applies vertical
168 mixing until static stability is restored. The second criterion is based on the Bulk Richardson number, which represents
169 wind-driven mixing. The mixed layer deepens until the Bulk Richardson number ($R_{ib} = (g\Delta\rho h)/(\rho_0(\Delta U)^2)$) reaches or
170 exceeds the critical values 0.6. The final criterion is the Gradient Richardson Number $R_{ig} = N^2/(\partial U/\partial z)^2$ which accounts for
171 shear instability. When $R_{ig} < 0.25$, local vertical mixing is applied. The PWP model is initialized with the ERA-5 12-hour
172 dataset of wind stress, heat, and freshwater fluxes (Hersbach et al., 2020) and the summer/winter averaged vertical
173 profiles of temperature and salinity from the observations presented here (Fig. S1-S3). The 1D model allows us to address
174 the relative contributions from diurnal heating/cooling, freshwater fluxes, and wind mixing.

175
176 In addition, we broaden the impact of our findings by using the hydrographic database published in Brakstad (2023)
177 that includes, in addition to the dataset from the Marine and Freshwater Research Institute of Iceland, other multiplatform
178 observations like Argo floats or cruise data between 1950 and 2019. For this objective, a larger oceanic region is used and
179 classified into α -ocean and β -ocean using the spice frequency, K^2 , (Carmack, 2007; Strehl et al., 2024), defined as:

180 $K^2 = N_T^2 - N_S^2$. (5)

181 K^2 is positive in α -oceans and negative for β -oceans.

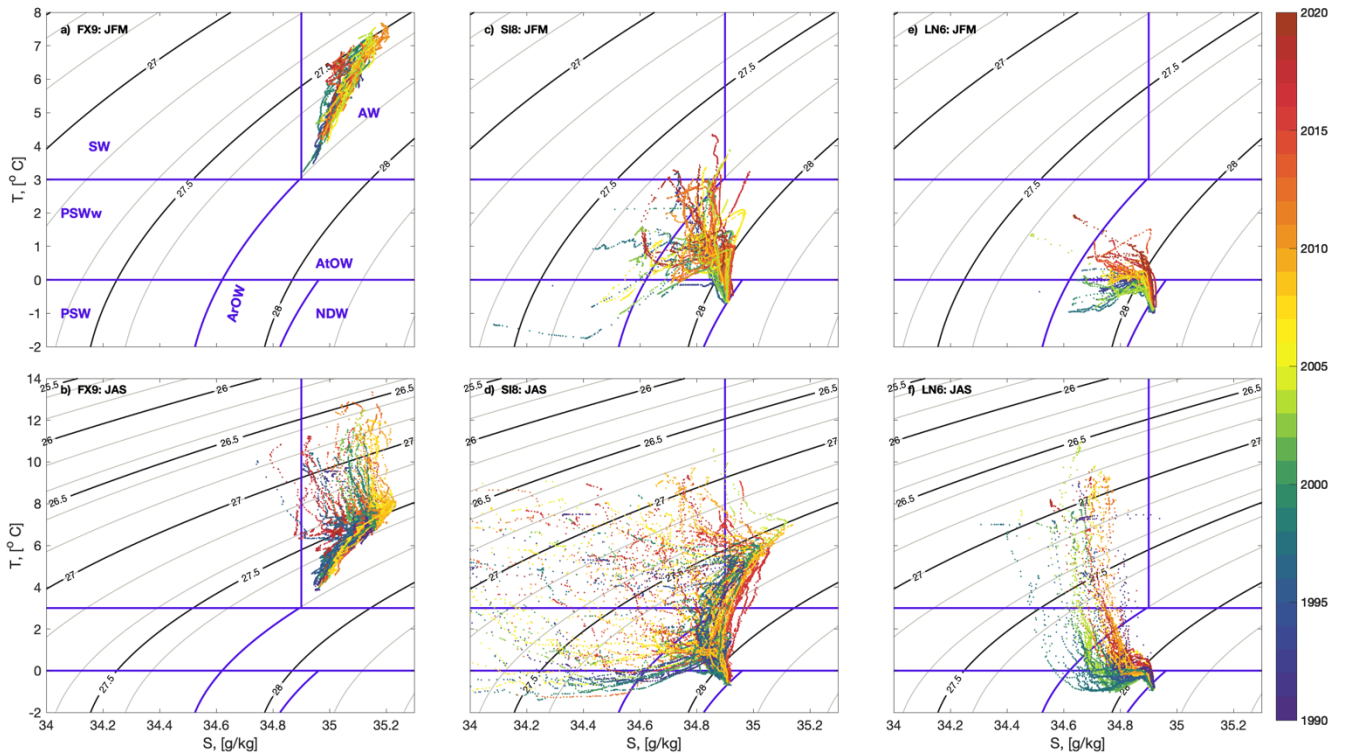
182

183 **3 RESULTS**

184 **3.1 Hydrographic properties around Iceland**

185 The hydrographic properties (potential temperature-salinity diagrams) around Iceland show important spatial, seasonal,
 186 and interannual variability (Figure 2); the T/S properties differ widely between the three representative stations: FX9, SI8
 187 and LN6 for the west, north and northeast of Iceland. FX9, in the southwest of Iceland, is completely dominated by Atlantic
 188 Water (AW; Fig. 2 a and b). At SI8, in the north, the dominating water masses in winter are of polar origin, i.e., warm Polar
 189 Surface Water (PSWw) in the upper layers, and Atlantic Overflow Water (AtOW) and Arctic Overflow Water (ArOW) in
 190 the intermediate/bottom waters (Fig. 2c and d). The SI8 station also presents the largest variance of its thermohaline
 191 characteristics. It is noteworthy that using fixed definitions of water masses may lead to biased estimates, as these water
 192 masses have been steadily warming over the past two decades. LN6, in the northeast, contains the coldest and densest
 193 waters on average (Fig. 2c and f).

194



195 **Figure 2: (Top row) Winter (JFM) and (bottom row) summer (JAS) T-S diagrams for three selected stations (a, b) FX9, (c, d) SI8**
 196 **and (e, f) LN6, considered as representative for the south, north and northeast regions shown in Fig. 1. The T-S individual profiles**
 197 **are color-coded by year. The main water masses as defined in Table 2, are labeled in panel (a).**
 198

199 The three stations have a clear seasonality. Overall, due to seasonal warming of the upper layers, the summer profiles
 200 span a wider temperature range (Fig. 2b, d, f) than in winter (Fig. 2a, c, e). FX9 is notably warmer and saltier than the other
 201 stations, especially in summer (Fig. 2a), when the minimum temperature in FX9 (nearly 4°C) is as high as the maximum
 202 temperature in SI8 and 2 degrees higher than in LN6 (Fig. 2a, b, c). At SI8 a large change in density between seasons is

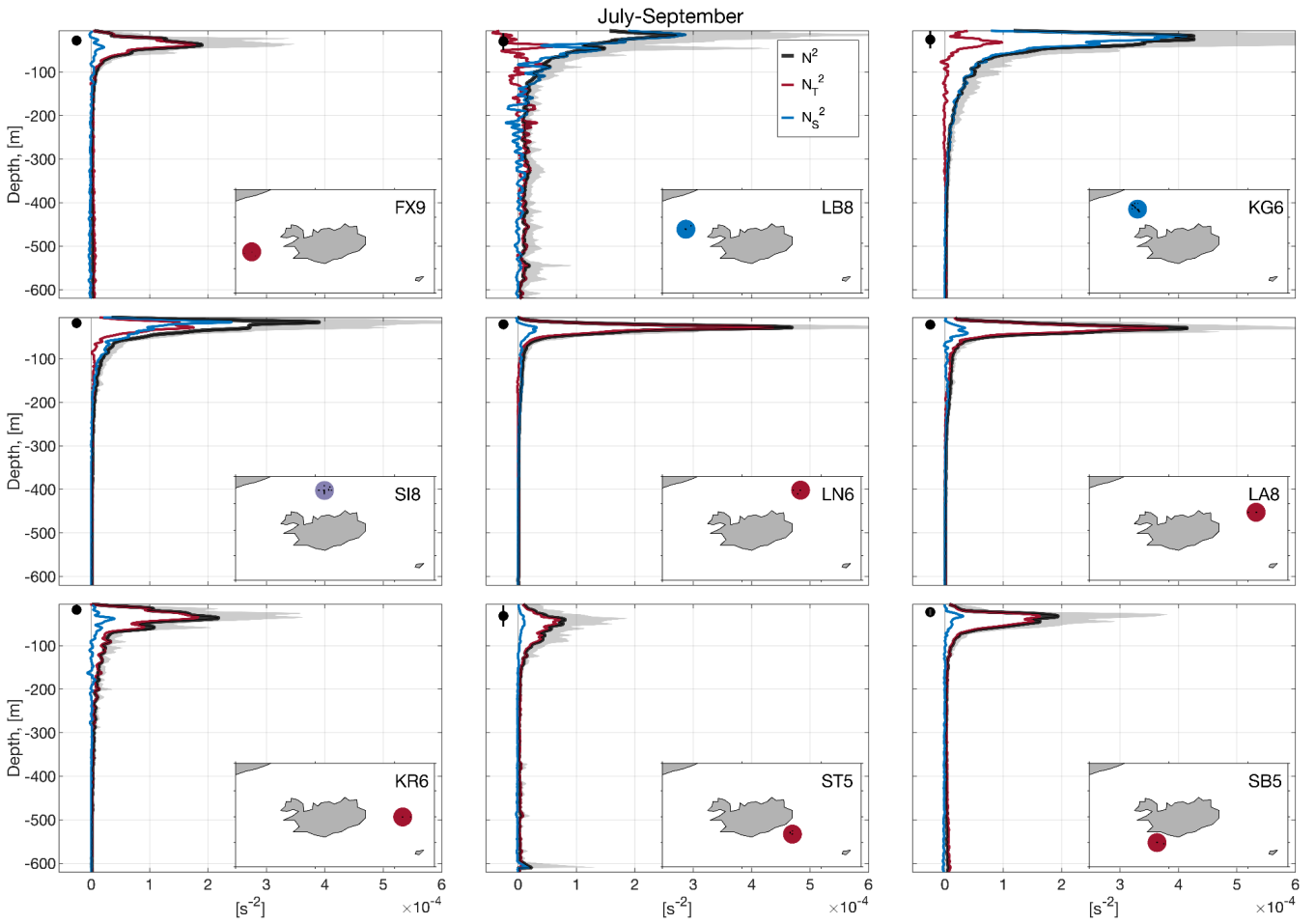
203 observed mainly driven by the contribution of AW, explained by offshore migration of the NIIC and the stronger inflow of
204 AW during the summer (Fig. 2c, and f) (Jónsson and Valdimarsson, 2012). While the widest seasonal amplitude in salinity
205 is observed at SI8, the largest seasonal amplitude in temperature is observed at LN6.

206 FX9 does not show a clear interannual pattern in summer, but in winter the 2000's are strikingly saltier than the other
207 years. In contrast, at SI8 and LN6 fresher and colder waters are observed in the 90's, they progressively warm and become
208 saltier over time, and they reach their maximum temperature and salinity by 2015-2018. This decadal pattern is more
209 evident in winter, but it is observed in both seasons.

210 **3.2 Seasonality of Stratification and Mixed Layer Depth (MLD)**

211 The spatial and temporal variability of the stratification around Iceland is remarkably large (Fig. 3 and Fig. 4), and the
212 relative contribution of temperature and salinity shows a strong seasonal cycle. In summer, the MLD is relatively shallow,
213 oscillating around 50 m with a small standard deviation (Fig. 3). In contrast, in winter the ML reaches depths greater than
214 400 m in FX9, ST5 and SB5 with large standard deviations spanning a 100 m range (Fig. 4). The deepest average MLD is
215 found in FX9 while the shallowest are KG6, SI8, LA8 and KR6.

216 In summer (Fig. 3), the upper-ocean stratification around Iceland (Fig. 3) is generally dominated by temperature, except
217 for the three northwestern stations (namely LB8, KG6, SI8). LB8 exhibit the largest variability in both N_T^2 and N_S^2 , but is
218 mainly dominated by salinity in the upper 200 m and by temperature below that depth. This transition station is located at
219 the sill of Denmark Strait, a convergence zone for several currents (see Table 1 and Fig. 1) carrying water masses with
220 contrasting T-S properties within the ML and the thermocline (Jónsson, 1999; Logemann et al., 2013; Casanova-Masjoan
221 et al., 2020). In KG6, the fresh inflow from the EGC compensates for the cold temperature, and salinity largely dominates
222 stratification. For SI8, we observe a mixed regime with almost equal contributions from both salinity and temperature to
223 the total stratification, which suggests that this is also an area of transitional regime. For the stations: LN6, LA8 and KR6,
224 despite the fact that stratification is mainly dominated by temperature, exhibit a small subsurface contribution of salinity
225 just below the ML, likely due to the presence of fresh PSWw. The southern stations ST5 and SB5, have a minimal
226 contribution to stratification from salinity, which may be associated with the numerous river discharges and the proximity
227 to the continental shelf. The river discharge is the largest near SB5, likely explaining the summer subsurface contribution
228 to salinity (Whitney, 2025).



229

230

Figure 3: Summer (JAS) average density stratification (N^2) profiles for the selected stations; the average total stratification (black) is decomposed into temperature (red) and salinity (blue) contributions, while the gray shaded band represents all the stratification profiles. The black solid dot (left of the profiles) represents the average MLD with the error bar showing the standard deviation as an indicator of the temporal variability. The maps in the lower corner show the location of the station within a circle color coded by the dominating regime according to the contribution to stratification: red for temperature, blue for salinity, and purple for a mixed regime.

235

236

The hydrographic conditions are very different for winter; the stratification is one order of magnitude lower, i.e., comparing Figure 3 and Figure 4. Also, the water temperature is much colder due to winter heat loss. Under these conditions, the relative contribution of salinity to the total stratification stands out around Iceland except at the southern stations (FX9, SB5, ST5), where the weakest winter stratification is observed. This southern region shows the deepest MLD, between 350 and 700 m in the stations FX9, SB5 and ST5, while for the northern stations (KG6, SI8, LN6, LA8, and KR6) the mean winter MLD is about 100 m. Similar to summer, station LB8, also shows high variability in winter stratification, associated with the confluence of currents at the Denmark Strait.

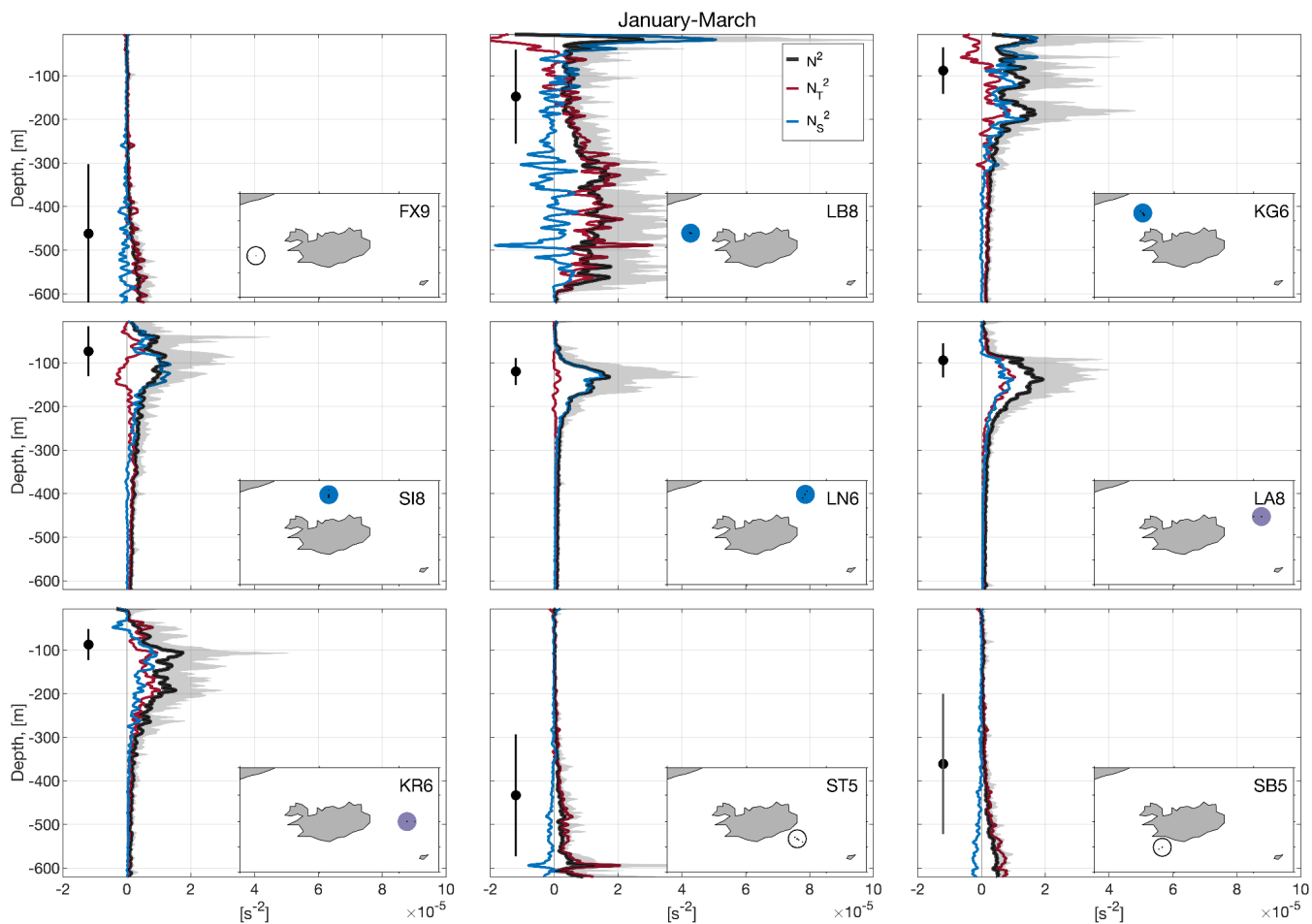
242

243

The role of temperature or salinity in setting the stratification (α - and β - ocean, see *e.g.*, Carmack, 2007) is linked to the hydrographic characteristics (temperature and salinity) of the dominant water masses within each region. Based on this, we can classify the waters around Iceland. The southern side is an α -ocean as it receives the influence of warm and relatively salty AW. Hence, the stratification is mainly temperature driven in both seasons (see FX9, ST5 and SB5 in Figures 3 and 4) and MLD gets deeper than 400 m in winter. The northwest of Iceland (LB8, KG6) is under the influence of the EGC throughout the year bringing fresh PSW and PSWw into the area. Therefore, this area with winter MLDs of 100-150 m can be considered a β -ocean, with heat fluxes equivalent to the southern region but with stronger and salinity dominated stratification blocking the potential for deep convection, i.e., this region does not have a mechanism to lose surface buoyancy seasonally in the salinity component. In contrast, the northeastern Icelandic area (SI8, LN6, LA8 and KR6) shifts

251

252 from β in winter to a mixed α/β in summer. This is likely due to an offshore migration of the NIIC increasing the inflow of
 253 AW (Jónsson and Valdimarsson, 2012; Casanova-Masjoan et al., 2020, their Figure 11). For instance, in winter, SI8 has a
 254 PSW signature at the thermocline with salinity driving the stratification and a MLD of about 90 m (β -ocean), and in summer,
 255 the NIIC brings warm AW to the upper layers of SI8 making the stratification similarly driven by temperature and salinity.
 256 Overall, the north of Iceland exhibits the strongest summer stratification of the study area which results in very shallow
 257 MLDs.



258
 259 **Figure 4: Same as Figure 3 but for winter (JFM). The white color circles shown in the maps of stations ST5, SB5, and FX9 indicate**
 260 **very weak winter stratification with no significant contribution of salinity or temperature.**

261 3.3 Interannual to decadal variability of the mixed layer properties

262 To investigate the interannual to decadal ML variability we focused on three reference stations, considered representative
 263 of the α -ocean (FX9, west), transition (SI8, north) and β -ocean (LB8, northwest) regimes around Iceland. FX9 dominated
 264 by relatively warm and salty AW, SI8 as a transition area, and LB8 dominated by cold and fresh PSW. The three stations
 265 show strong interannual variability.

266 In FX9, to the west of Iceland, there is a correlation ($R=0.69$ p -value <0.01) between mixed layer temperature (MLT) and
 267 salinity (MLS) anomalies. Between 1990 and 1998 the mixed layer was the deepest, the coldest, and the second freshest
 268 period, as shown in Figure 5a, and d (positive MLD anomalies correspond to deeper ML and negative ones correspond to
 269 shallower ML). Around the period 2000-2014, there is an increase in MLT and MLS as the ML becomes moderately
 270 shallower. The winter MLD is the shallowest, saltiest, and warmest in 2010 (Fig. 5a, and d), when the temperature
 271 contribution seems to control this minimum. From 2015 to 2018 the ML returns to the cold and fresh conditions of the 90's
 272 but the MLD is near its long-term average. The observed variability of the ML and its temperature in FX9 exhibits
 273 correlation (R) with the North Atlantic Oscillation (NAO); for MLD, the best correlation was $R=0.53$, p -value <0.01 at lag

274 zero; for MLS $R=-0.52$, $p\text{-value}<0.01$ at lag -2 years (NAO leading), and for MLT $R=-0.49$, $p\text{-value}<0.01$ at lag -1 year
 275 (NAO leading (Fig. 5g, h). However, in our assessment, the 2-year lag lacks a plausible physical explanation; therefore, we
 276 do not consider it a reliable correlation. More qualitatively, positive NAO at the beginning and the end of the time series,
 277 corresponds with deeper, colder, and fresher MLs, while negative NAO between 2000 and 2015 roughly corresponds with
 278 shallower, warmer, and saltier MLs. As shown in Figure 2, FX9 contains only AW (Fig. 2a, d) likely advected from the
 279 south to the area by the Gulf Stream and later the Irminger Current. Similar conditions have been observed in the Irminger
 280 Sea over the same period, and they have been related to the NAO phase and its impact on the Subpolar gyre (Feucher et
 281 al., 2022). This suggests that the FX region is largely influenced by the Atlantic climate and therefore it is partly impacted
 282 by the NAO (Bersch, 2002).

283 At SI8, in the north of Iceland (Fig. 5b, e, h), the negative winter MLD anomalies are on the order of those at FX9 and
 284 also exhibit strong interannual variability without an identifiable pattern. Strong positive MLD anomalies are observed in
 285 particular years (e.g., 2000, 2007, and 2016), but they do not seem correlated with the MLT/MLS or with the NAO
 286 variability. Interestingly, the MLT and MLS co-vary during the period 1990-2005, when the mixed layer is colder and
 287 fresher, but this correlation weakens from 2005 to 2018, when the positive MLT anomalies increase while the MLS
 288 anomalies, although positive, do not vary significantly.

289 In LB8 (northwest), the winter MLD has the largest variability as the station is located in the vicinity of the front between
 290 NIIC and the EGC, which shapes the Polar and Atlantic conditions. Despite this large variability, a co-variance between
 291 MLT and MLS anomalies seems to be correlated with the position of the front. Fresher and colder MLs are associated with
 292 EGC influence and warmer/saltier MLs with the presence of NIIC (Fig. 5c, f, i). Generally, shallower MLs are also fresher
 293 and colder, which agrees with a salinity-dominated stratification in the upper layer (Fig. 4b). Three particular years present
 294 relatively deep, cold, and salty MLs: 1996, 2006 and 2014. The observed interannual variability in the ML and its properties,
 295 while large, does not seem to be correlated with the NAO, except during the last decade, when the high state of the NAO
 296 is consistent with the positive MLT and MLS, suggesting a larger presence of the NIIC at this station.

297



298
 299

300 **Figure 5: Interannual winter (JFM) variability from 1990 to 2019 in three stations representative of different regions around**
 301 **Iceland: (a, b, c) MLD anomaly (in percentage of its mean winter value over the whole record, green shading) and mixed layer**
 302 **temperature (MLT, blue bars). (d, e, f) Mixed layer salinity (MLS, grey bars) and winter average NAO index for comparison (purple**
 303 **shading). (g,h,i) Mixed layer density anomaly (MLrho, red bars) and Mixed layer density (kg/m^3), black dots. The represented**
 304 **stations are (a, d) FX9, in the southwest, (b, e) SI8, in the north, and (c, f) LB8 in the northwest. Positive anomalies in MLD, MLS,**
 305 **MLT, and MLrho correspond to deeper, saltier, warmer, and denser waters, respectively. The summary of the correlations is**
 306 **presented in Table 1.**

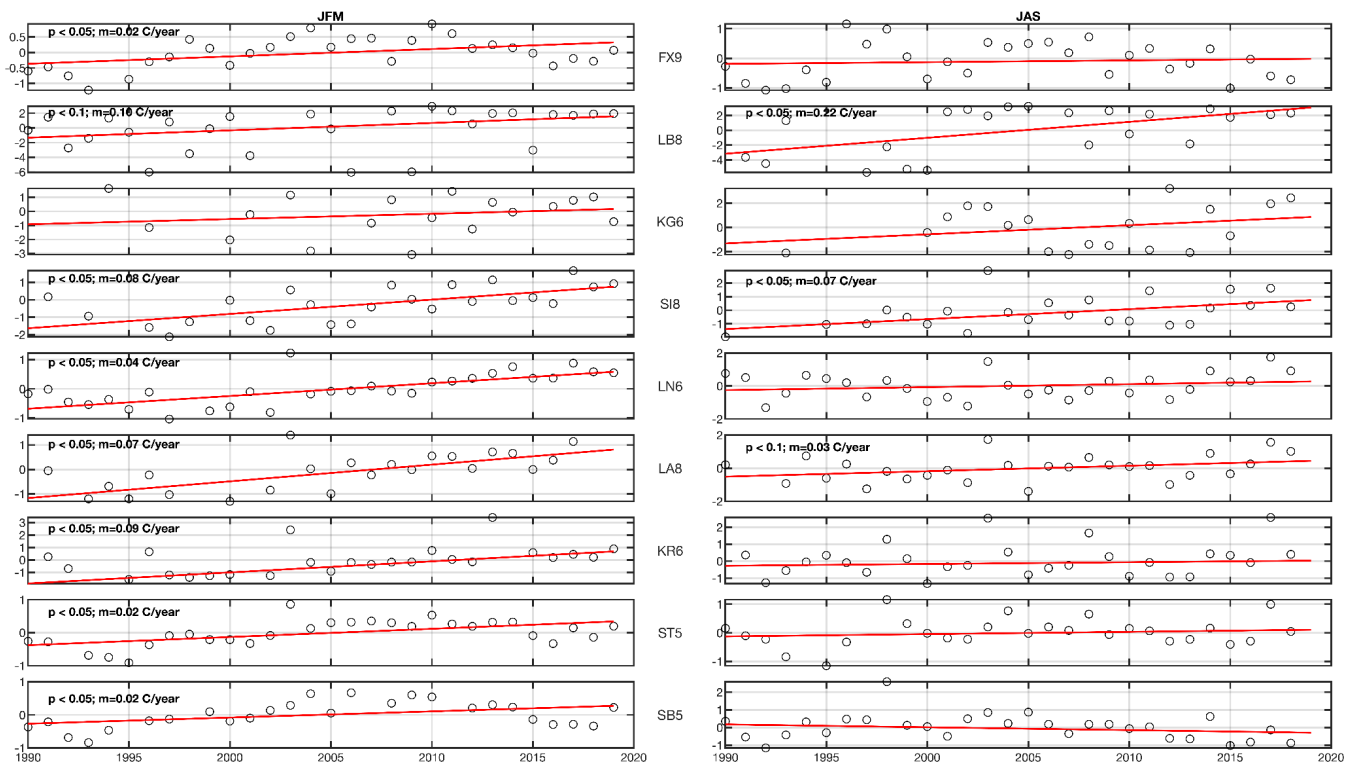
307 *Table 1. Summary of the Pearson correlation coefficients between the different variables shown in Figure 5. Non-significant correlations*
 308 *are omitted. The displayed correlations are significant at 95% confidence ($p < 0.05$), and those significant at 99% ($p < 0.01$) are shown in*
 309 *bold.*

	FX9		SI8		LB8	
	Correlation	p-value	Correlation	p-value	Correlation	p-value
MLT-MLS	R=0.69	p<0.01	R=0.74	p<0.01	R=0.95	p<0.01
MLT-MLD	--	--	--	--	R=0.76	p<0.01
MLS-MLD	--	--	--	--	R=0.68	p<0.01
NAO-MLD	R=0.53	p<0.01	--	--	--	--
NAO-MLT	R=-0.41	p<0.003	--	--	--	--
NAO-MLS	--	--	--	--	--	--

310

311 To delve into the interannual to decadal variability of the MLT around Iceland, we analyzed its anomalies (relative to the
 312 long record) in all nine stations and computed their linear trends (Fig. 6). The temperature anomalies show significant
 313 interannual variability and spatial differences around Iceland. For instance, positive anomalies were observed in 2003 in
 314 most of the stations in both seasons, with particularly large temperature anomalies east of Iceland. Strong warm anomalies
 315 are also observed in 2017, mostly in summer at all stations except FX9 and SB5, located south of Iceland (Fig. 6; left panel).
 316 Although the 29-year period might be too short for identifying linear anthropogenically-driven trends, linear trends are
 317 significant in some of the stations, (where the p-value is indicated). The linear trends show a general warming of the mixed
 318 layer that is more evident in winter, mainly in the stations of the northeast (LN6, LA8). In the south (ST5, SB5 and FX9),
 319 even if the trend is significant from 2000-2015, there is an interannual variability that induces colder mixed layer conditions
 320 from 2015 to 2018. This tendency of returning to the conditions observed in the early 90's may be associated with the NAO
 321 (Feucher et al., 2022) as shown in Fig. 5. The observed general warming of the ML around Iceland is consistent with the
 322 progressive warming of the NIIC (Casanova-Masjoan et al. 2020).

323

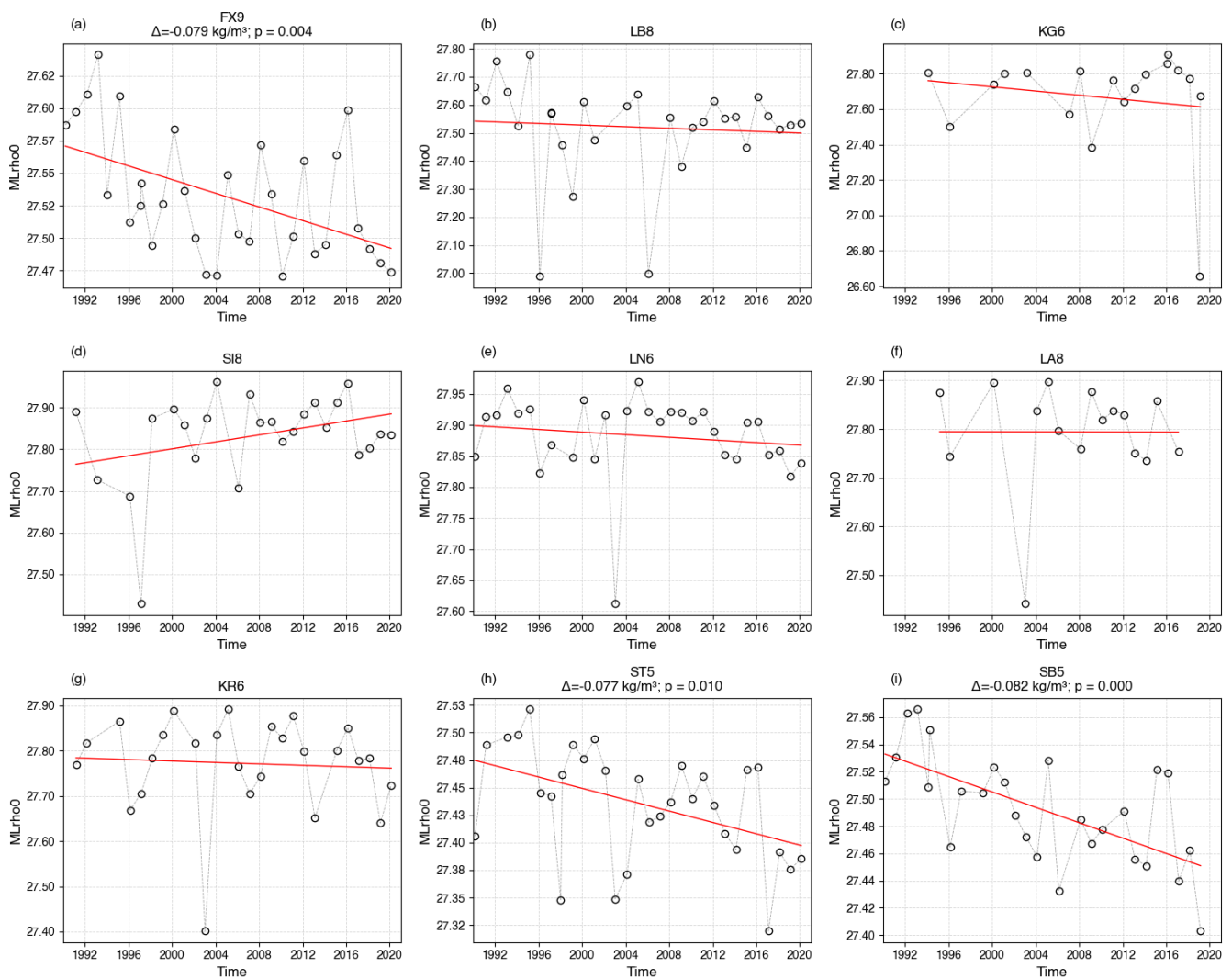


324
325
326
327

Figure 6: Mixed Layer Temperature (MLT) anomaly time series (left) winter (JFM) and (right) summer (JAS) for the 9 stations shown in Figures 3, 4. The anomalies show the p-values and the linear trends.

328
329
330

Similarly to Figure 6, in Figure 7 we compute the winter (JFM) density within the ML, which exhibits a statistically significant decrease for the stations in the south of Iceland (FX9, SB5, and ST5). The rest of the stations around Iceland do not show any significant changes. Remarkably, LN6, LA8, and SI8 show no change in density even though they experience a significant increase in temperature.



331

332 **Figure 7: Mixed layer density (Mlrho) time series for the 9 representative stations only for winter (JFM). Stations FX9, ST5, and**
 333 **SB5 exhibit a statistically significant negative trend, with a total accumulated value of $\Delta \sim -0.08$ kg/m³ over the 29 years of**
 334 **observations.**

335 **4 . MLD driving mechanisms from a 1D model**

336 The stratification around Iceland in summer is roughly an order of magnitude higher than in winter, largely due to
 337 positive buoyancy forcing, resulting in shallower and more variable MLDs. Therefore, we study the atmospheric effect
 338 on these α - and β -ocean regions by implementing the Price et al. (1986) one-dimensional model. The model is forced
 339 starting in the fall before the deep MLD develops. The model results of the MLDs shown in Figure 8 are within the range
 340 of the observed average \pm standard deviations (thick black dots and lines in Fig. 8). For most stations a spring shoaling of
 341 the MLD is driven by reduced heat fluxes, while the MLD remains relatively deep due to the wind-stress.

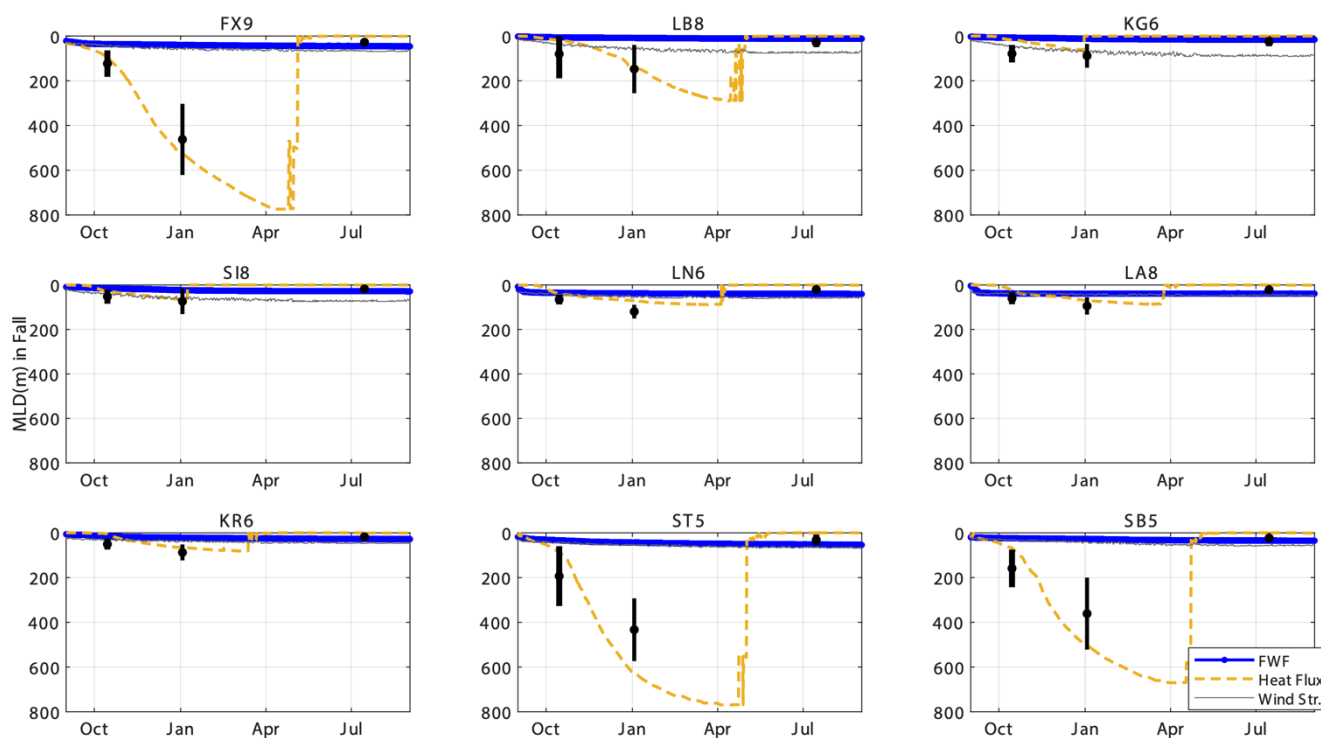
342 In the model, the stations embedded within the α -ocean with AW (Fig. 8: FX9, SB5 and ST5) present the largest MLDs
 343 exceeding 300 m depth, which is consistent with the observations. In this α -ocean region, the development of a deep ML
 344 is driven mainly by heat. However, within these stations, the wind-stress steadily contributes to the development of the ML.
 345 During the summer, shoaling of the mixed layer is likely influenced by the changes of both heat and freshwater fluxes, with
 346 their effects on the MLD partially offset by wind stress (Fig. 8: FX9, SB5 and ST5).

347 The station LB8, despite being in Denmark Strait and presenting a large contribution of PSWw and PSW in the upper

348 layers (driving a β -ocean stratification), shows that the development of MLDs can be influenced by both, heat flux and/or
 349 wind stress (Fig. 8: LB8). However, the contribution of wind-stress and freshwater cannot lead to MLDs deeper than
 350 100m (Fig. S4:LB8). Beneath the PSW and PSWw at LB8 we find AtOW. Hence as the wind-stress develops, the MLD
 351 evolution erodes the PSWw strata reaching the AtOW layer, allowing reduced heat fluxes to contribute to the MLD
 352 development. This erosion is not visible on the stations embedded within the EIC.

353 Wind stress becomes the leading forcing mechanism northeast of LB8 at stations KG6, and SI8, coinciding with the shift
 354 from α - to β - ocean stratification (Fig. 8). This region has a lower convective potential than regions with pure AW and
 355 therefore does not produce large MLDs (Fig. 4 and 8). The MLD there results from roughly equal contributions of
 356 convection and wind-driven mixing. At these stations, the best performance of the PWP model is obtained when both heat
 357 flux and wind-stress are included (Fig. S4). Notably, the summer MLD remains shallow and is roughly the same order of
 358 magnitude across all stations around Iceland (Fig. 8 and S4).

359



360

361 **Figure 8: MLD driving mechanism decomposition estimated from the PWP 1-D model (Price et al. 1986) for each of the studied**
 362 **stations. Different MLD evolutions are shown for outputs forced with freshwater fluxes (blue), heat fluxes (red), and wind-stress**
 363 **(grey). Black dots represent the mean fall, winter, and summer MLDs with their corresponding standard deviations (black lines).**

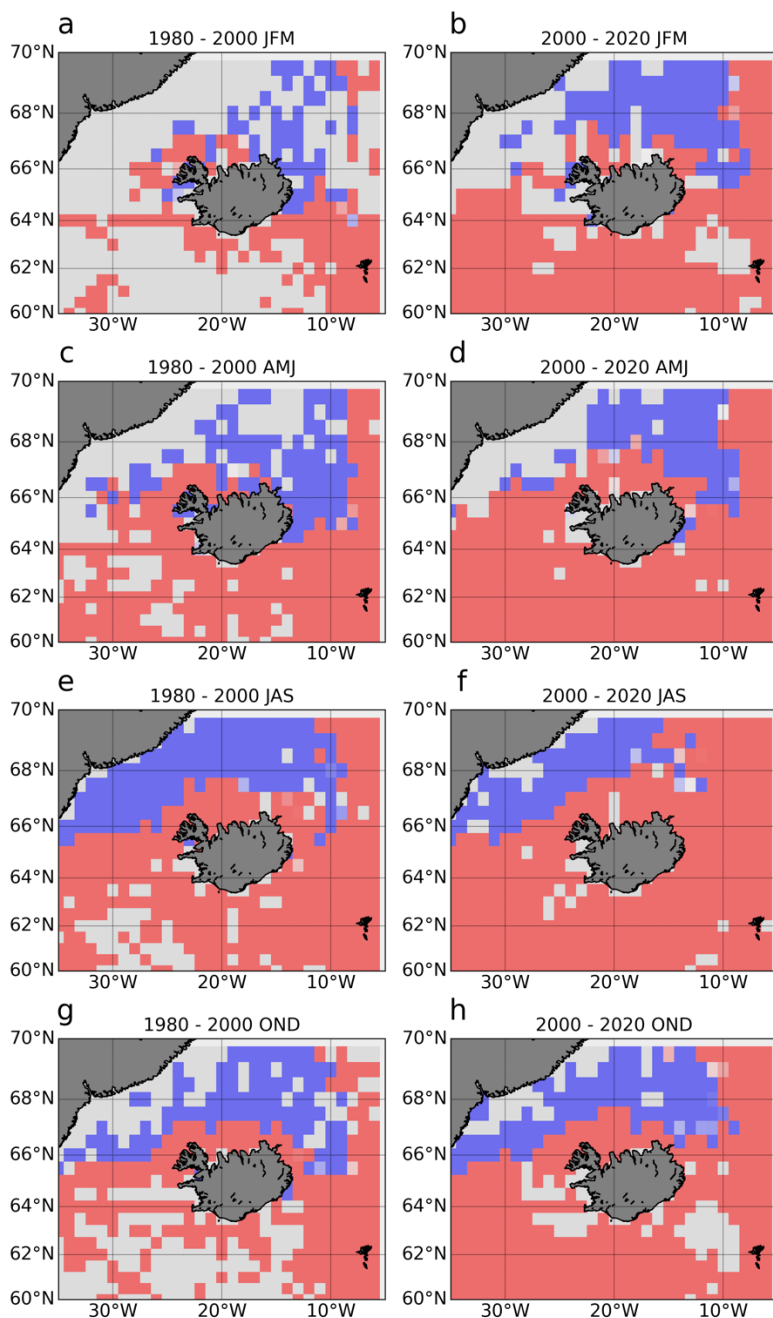
364

365

366 5. Stratification around Iceland

367 To complement the understanding of the stratification of the Arctic and Subarctic waters around Iceland, their connection
 368 with water masses, currents, and their variability, we used the spice frequency averaged in the first 200 m, estimated
 369 following the methods described in Strehl et al. (2024) implementing Equation (5). For this analysis we used the
 370 hydrographic dataset in Brakstad et al (2023). The spiciness distributions shown in Figure 9 reveal that temperature

371 dominates on the southern side of Iceland, marked by an α -ocean regime, while salinity dominates the northern side,
372 associated with β -ocean. These areas largely correspond with the distribution of AW versus PSW/PSWw (See Fig. 2 for
373 T-S definitions).



374
375 **Figure 9: Mean upper 200m spice frequency for the region of study showing the α -ocean (red) and β -ocean (blue) regions for the**
376 **periods of 1980-2000 and 2000-2020 and the four main seasons JFM (a,b), AMJ (c,d), JAS (e,f) and OND (g,h). The Brakstad et al**
377 **(2023) hydrographic dataset is used for this calculation.**

378 The seasonal distribution of spice frequency north of Iceland agrees with the seasonal behavior of the NIIC described in
379 Casanova-Masjoan et al. (2020) where the NIIC surface extension in winter and spring remains constrained to the northwestern
380 side of Iceland due to the cold southeast surface imprint of the EIC. In summer, the NIIC expands northeastward, reaching all
381 the way to the eastern side of Iceland and the northernmost station at the SI transect and constraining the polar water between
382 the northern end of the Kolbeinsey Ridge and the Greenland shelf. In fall, the NIIC northern extension narrows but is still able
383 to surround Iceland. It is noteworthy that a clear increase in coverage of the α -ocean, mainly in summer, is observed by
384 comparing the 1980-200 average and the 2000-2010 average.

386 In this study, we discussed the seasonal and interannual variability of the mixed layer characteristics and the stratification
387 regimes around Iceland by using a long time series of CTD data. Based on our results, we propose the regionalization of
388 the waters around Iceland into three dynamical regions α -ocean, β -ocean, and transition-ocean.

389 The southwestern region is dominated by AW both in winter and summer. Within this region, the winter MLD
390 is the deepest and most variable of the whole study area, with ML's occupied by AW over the whole sampling period.
391 This region is influenced by the dynamics of the Irminger Sea and the Subpolar gyre and has favorable conditions (α -
392 ocean) for winter deep convection driven by heat fluxes to develop deep mixed layers, which agrees with previous
393 studies (Carmack, 2007; Våge et al., 2008; Piron et al., 2016; Stewart and Haine, 2016; Petit et al., 2020). In the
394 southern region, the ML salinity anomaly was negative over the last 5 years, which is consistent with previous
395 numerical models and Argo observations showing a freshening trend of the North Atlantic (Tesdal et al., 2018;
396 Holliday et al., 2020, Liu et al., 2020). However, since the south of Iceland is an α -ocean, these recent changes have
397 not yet reached or affected the MLD.

398 The northwestern region, which includes the Denmark Strait, is a medley of all the water masses described in this study.
399 In this region there is a confluence of Greenland shelf and slope waters and Iceland Sea origin waters (Harden et al., 2016;
400 Foukal et al., 2020). This includes the NIIC generating an important variability in the water properties due to complex
401 interactions of the regional currents (Lin et al. 2020, Mastropole et al. 2017). The MLD variability over time at the KG6
402 and LB8 stations is moderate (<100m), except for the years 2000, 2007 and 2016 when the ML was anomalously deep. In
403 this region, the stratification is notably year-round dominated by salinity (β -ocean), which is explained by the strong Polar
404 influence of cold and fresh waters transported by the EGC. A broader look into the northwestern side of the basin reveals
405 that this area can be divided at the center of the Denmark Strait into an α -ocean near the Icelandic shelf where the NIIC
406 flows and a β -ocean as we progress towards Greenland (where the LB8 and KG6 stations are located). Near the Icelandic
407 shelf, MLDs are driven mainly by wind-stress, with a secondary contribution of heat fluxes. The T-S properties as well as
408 the MLT anomalies in the northwest region near the Icelandic shelf show that the NIIC waters there are getting warmer and
409 saltier. This agrees with previous studies showing the transformation of the NIIC also accompanied by an increase in its
410 transport with time (Casanova-Masjoan et al., 2020). Even if the α -ocean area is warming, it is not expanding
411 northwestward. This suggests that the EGC may act as a barrier, bringing PSW into the region and maintaining the β -ocean
412 state on the northwesternmost side of the strait. This β -ocean, where the MLD is shallow all year round has dynamical
413 implications as the strong shallow stratification inhibits baroclinic instability and eddy generation (de Marez et al., 2025).

414 Northeast of Iceland, the ML exhibits intrusions of SW in the winter, while AW is present during the summer. In this
415 region, the stratification changes from β - to α -ocean seasonally. The Kolbeinsey Ridge acts as a barrier where we find the
416 eastward penetration of the EIC bringing fresh waters (PSWw) from the East Greenland Current (Macrander et al., 2014;
417 Casanova-Masjoan et al., 2020). In summer, the NIIC expands northeastward, bringing AW into the area and changing the
418 stratification regime to α . Hence, the mixed layer waters show important seasonal variability. They range from maximum
419 temperature below 2 °C in winter to over 10 °C in summer. This is also the only region where a significant warming decadal
420 trend emerges over the interannual variability and progressively results in a stronger α -ocean. This agrees with the AW
421 warming observed in Casanova-Masjoan et al. (2020) and with the northward progression of AW named as 'Atlantification'
422 described by Polyakov et al. (2017). This shift to α -ocean or 'Atlantification' may lead to deeper ML's (Moore et al., 2015;
423 Våge et al., 2022), and the associated deeper convection may increase the potential of this area to contribute to the dense
424 flow carried by the NIJ (Semper et al. 2019).

425 The regionalization proposed in this work, based on hydrographic properties, matches the recently proposed distribution
426 of primary production around Iceland (Richardson and Bendtsen, 2021; Cerfonteyn et al., 2023), supporting the importance
427 of MLD properties for the primary production (Ólafsson, 2003). The induced alterations on primary production can lead to
428 ecosystem changes. For example, Iceland has witnessed a rapid increase in the population of mackerel, a relatively warm-
429 water fish, since 2006 (Asthórsson et al., 2012; Campana et al., 2020) starting from the southeast towards the north, and
430 recently they have been reported almost all around the country. This migration is consistent with our of both the increase
431 in surface temperatures, i.e., northward shift of warmer isotherms over the Iceland Faroe Ridge (de Marez et al., 2025) and
432 the increase of temperatures within the ML in the same regions over the last decade, which may establish new pathways
433 for entire ecosystems.

434 The long time series investigated here revealed important interannual oscillations of the ML properties. Five main
435 features are to be highlighted: (i) We do not observe any linear trend in the MLD, which is rather subject to strong
436 interannual variability. (ii) Except for the southern stations, influenced by the subpolar gyre, the interannual variability was
437 not correlated with the NAO. For example, FX9 shows a significant negative of MLT with the NAO ($R=-0.41$ and p -value
438 < 0.03). (iii) The southern stations, FX9, SB5, and ST5, within the α -ocean region, show a clear decrease in ML density,
439 with statistically significant values and experience a total decrease during the 29-year period of -0.08 kg/m^3 . (iv) The linear
440 fit indicates significant (at 95%) warming trends in the MLT of most of the stations in winter, with the maximum trend of
441 $0.08 \text{ }^\circ\text{C/year}$ at SI8 resulting in approximately $2.2 \text{ }^\circ\text{C}$. This agrees with previous studies (Sarafanov, 2009) showing that
442 the northern part of the North Atlantic (south of Iceland) is strongly dominated by atmospheric interannual to decadal
443 variability, particularly, where AW is present. The exception here is the northeastern region of Iceland where we observe
444 a clear warming trend of the ML (2010-2020). (v) We observe an ‘Atlantification’ expressed as a northeastward progression
445 of the α -ocean state. This progression will highlight the role of the northeastern area of Iceland as a convective zone where
446 deep water could be formed and contribute to the NIJ.

447 AUTHOR CONTRIBUTIONS

448 Conceptualization, ARA, MDPH and EP; methodology, ARA, EP and MDPH; software, ARA and AP; formal analysis,
449 ARA, EP, TM, CdM and MDPH; investigation, ARA, EP and MDPH, AM; data acquisition, SRÓ and AM; data curation,
450 SRÓ and AM; writing—original draft preparation, ARA, EP and MDPH; writing—review and editing, SRÓ, AM and SJ,
451 TM; visualization, ARA and EP; project administration, SRÓ; funding acquisition, ARA and SRÓ. All authors have read
452 and agreed to the published version of the manuscript.

453 FUNDING

454 ARA and CdM have been supported by HM Queen Margrethe II’s and Vigdís Finnbogadóttir’s Interdisciplinary
455 Research Centre on Ocean, Climate and Society (ROCS) under grant no. 158-4223. Support for this work was also
456 provided by the European Union’s Horizon 2020 research and innovation programme under grant no. 727852, Blue-
457 Action project (AM and SJ). This work has been supported by the FAR-DWO (PID2020-114322RB100) project from the
458 Spanish Ministry of Research.

459 ACKNOWLEDGMENTS

460 We are grateful for the invaluable cooperation we have had with the crews of the Icelandic research vessels Bjarni
461 Sæmundsson and Árni Friðriksson and to the many people at the Marine Research Institute that have contributed to the

462 hydrographic observations over the years. ARA and MDPH would like to dedicate this paper to the memory of Maria
463 Casanova-Masjoan.
464

465 **Table 2.** Characteristics for the representative stations for each typical surveyed section. The representative ocean currents
 466 at each section are also shown: North Icelandic Irminger Current (NIIC), Irminger Current (IC), East Greenland Current
 467 (EGC), North Icelandic Jet (NIJ), East Icelandic Current (EIC), and North Atlantic Current. (NAC). The corresponding
 468 stratification regimes are listed for summer and winter for each station.

469
 470

Station	Depth, [m]	Lon	Lat	Oceanic region	Significant currents	Stratification regime
Faxaflói (FX9)	1010	-27.98	64.35	Subpolar North Atlantic	IC	Alpha-ocean (summer) Weakly stratified (winter)
Látrabjarg (LB8)	658	-27.050	66.083	Denmark Strait	NIIC, EGC, DSO	Beta-ocean (all year round)
Kögur (KG6)	980	-23.933	67.583	Western Iceland Sea	EGC, DSO	Beta-ocean (all year round)
Síglunes (SI8)	1023	-18.83	68.00	Kolbeinsey Ridge	NIIC, EGC, EIC, NIJ	Transition (summer) Beta-ocean (winter)
Langanes NE (LN6)	1850	-12.66	68.00	Iceland Sea	EIC	Alpha-ocean (summer) Beta-ocean (winter)
Langanes E (LA8)	1251	-9.00	66.37	Iceland Sea	EIC	Alpha-ocean (summer) Transition (winter)
Krossanes (KR6)	1419	-9.00	65.00	Iceland Sea/ North Atlantic	EIC, NAC	Alpha-ocean (summer) Transition (winter)
Stokksnes (ST5)	1153	-13.66	63.66	North Atlantic	NAC	Alpha-ocean (summer) Weakly stratified (winter)
Selvogsbanki (SB5)	1006	-21.48	62.98	North Atlantic	IC	Alpha-ocean (summer) Weakly stratified (winter)

471
 472
 473
 474

Table 3. Main water masses definitions for the region of study (Rudels et al., 2005; Våge et al., 2011)

Water mass	Potential Temperature (θ)	Salinity	Potential density (σ_0 , kg m^{-3})
Surface Water(SW)	$> 3^\circ\text{C}$	-	$\sigma_0 < 27.70$
Warm Polar Surface Water (PSW _w)	$0^\circ\text{C} \leq \theta < 3^\circ\text{C}$	-	$\sigma_0 < 27$
Polar Surface Water (PSW)	$< 0^\circ\text{C}$,	-	$\sigma_0 < 27.70$

Atlantic Water(AW)	$> 3^{\circ}C$	> 34.9	-
Atlantic-origin Overflow Water (AtOW)	$0^{\circ}C \leq \theta < 3^{\circ}C$	-	$\sigma_0 \geq 27.8,$ $\sigma_{0.5} < 30.44$
Polar intermediate Water (PIW)	$0^{\circ}C$	≤ 34.676	$\sigma_0 > 27.70,$
Arctic-origin Overflow Water (ArOW)	$< 0^{\circ}C$	-	$\sigma_0 > 27.8,$ $\sigma_{0.5} < 30.44$
Nordic Seas Deep Water (NDW)	$< 0^{\circ}C$	-	$\sigma_{0.5} \geq 30.44$

475
476
477
478
479
480
481
482
483
484
485
486
487
488
489
490
491
492
493
494
495

496

498 **References**

- 499 Astthorsson, O. S., Valdimarsson, H., Gudmundsdottir, A., and Oskarsson, G. J.: Climate-related variations in the
500 occurrence and distribution of mackerel (*Scomber scombrus*) in Icelandic waters, *ICES J. Mar. Sci.*, 69, 1289–1297, 2012.
- 501 Athanase, M., Provost, C., Perez-Hernández, M. D., Sennechael, N., Bertosio, C., Artana, C., et al.: Atlantic water
502 modification north of Svalbard in the Mercator physical system from 2007 to 2020, *J. Geophys. Res.: Oceans*, 125,
503 e2020JC016463, <https://doi.org/10.1029/2020JC016463>, 2020.
- 504 Bachman, S. D., Taylor, J., Adams, K., and Hosegood, P.: Mesoscale and submesoscale effects on mixed layer depth in
505 the Southern Ocean, *J. Phys. Oceanogr.*, 47, 2173–2188, 2017.
- 506 Bindoff, N. L., Cheung, W. W., Kairo, J. G., Arístegui, J., Guinder, V. A., Hallberg, R., et al.: Changing ocean, marine
507 ecosystems, and dependent communities, IPCC Special Report on the Ocean and Cryosphere in a Changing Climate, 477–
508 587, 2019.
- 509 Brakstad, A.: Hydrographic and Geochemical Observations in the Nordic Seas Between 1950 and 2019, University of
510 Bergen, 2023b.
- 511 Bersch, M.: North Atlantic Oscillation–induced changes of the upper layer circulation in the northern North Atlantic Ocean,
512 *J. Geophys. Res.*, 107(C10), 3156, <https://doi.org/10.1029/2001JC000901>, 2002.
- 513 Campana, S. E., Stefansdottir, R. B., Jakobsdottir, K., and Solmundsson, J.: Shifting fish distributions in warming sub-
514 Arctic oceans, *Sci. Rep.*, 10, 1–14, 2020.
- 515 Carmack, E. C.: The alpha/beta ocean distinction: A perspective on freshwater fluxes, convection, nutrients and
516 productivity in high-latitude seas, *Deep Sea Res. Part II: Top. Stud. Oceanogr.*, 54, 2578–2598, 2007.
- 517 Carton, J. A., Grodsky, S. A., and Liu, H.: Variability of the oceanic mixed layer, 1960–2004, *J. Climate*, 21, 1029–1047,
518 2008.
- 519 Casanova-Masjoan, M., Perez-Hernández, M. D., Pickart, R. S., Valdimarsson, H., Ólafsdóttir, S., Macrander, A., et al.:
520 Along-stream, seasonal, and interannual variability of the North Icelandic Irminger Current and East Icelandic Current
521 around Iceland, *J. Geophys. Res.: Oceans*, 125, e2020JC016283, <https://doi.org/10.1029/2020JC016283>, 2020.
- 522 Cerfonteyn, M., Groben, R., Vaulot, D., et al.: The distribution and diversity of eukaryotic phytoplankton in the Icelandic
523 marine environment, *Sci. Rep.*, 13, 8519, <https://doi.org/10.1038/s41598-023-35516-w>, 2023.
- 524 Dai, A., Luo, D., Song, M., and Liu, J.: Arctic amplification is caused by sea-ice loss under increasing CO₂, *Nat. Commun.*,
525 10, 1–13, 2019.
- 526 de Boyer Montégut, C., Madec, G., Fischer, A. S., Lazar, A., and Iudicone, D.: Mixed layer depth over the global ocean:
527 An examination of profile data and a profile-based climatology, *J. Geophys. Res.: Oceans*, 109,
528 <https://doi.org/10.1029/2004JC002378>, 2004.
- 529 de Marez, C., Ruiz-Angulo, A., & Gula, J. Mesoscale induced vertical fluxes over the Iceland-Faroe ridge. *Geophysical*
530 *Research Letters*, 52(13), 2025.
- 531 de Marez, Charly, Clara R. Vives, Esther Portela, and Angel Ruiz-Angulo. Mesoscale ocean processes: The critical role
532 of stratification in the Icelandic region. *Journal of Geophysical Research: Oceans* 130, no. 6 (2025).
- 533 Feucher, C., Portela, E., Kolodziejczyk, N., & Thierry, V. Subpolar gyre decadal variability explains the recent

534 oxygenation in the Irminger Sea. *Communications Earth & Environment*, 3(1), 279, 2022.

535 Foukal, N. P., Gelderloos, R., and Pickart, R. S.: A continuous pathway for fresh water along the east Greenland shelf, *Sci.*
536 *Adv.*, 6, eabc4254, 2020.

537 Fox-Kemper, B., H.T. Hewitt, C. Xiao, G. Aðalgeirsdóttir, S.S. Drijfhout, T.L. Edwards, N.R. Golledge, M. Hemer, R.E.
538 Kopp, G. Krinner, A. Mix, D. Notz, S. Nowicki, I.S. Nurhati, L. Ruiz, J.-B. Sallée, A.B.A. Slangen, and Y. Yu, 2021:
539 Ocean, Cryosphere and Sea Level Change. In *Climate Change 2021: The Physical Science Basis. Contribution of Working*
540 *Group I to the Sixth Assessment Report of the Intergovernmental Panel on Climate Change* [Masson-Delmotte, V., P. Zhai,
541 A. Pirani, S.L. Connors, C. Péan, S. Berger, N. Caud, Y. Chen, L. Goldfarb, M.I. Gomis, M. Huang, K. Leitzell, E. Lonnoy,
542 J.B.R. Matthews, T.K. Maycock, T. Waterfield, O. Yelekçi, R. Yu, and B. Zhou (eds.)]. Cambridge University Press,
543 Cambridge, United Kingdom and New York, NY, USA, pp. 1211–1362, doi: 10.1017/9781009157896.011.

544 Gjelstrup CVB, Sejr MK, de Steur L, Christiansen JS, Granskog MA, Koch BP, Møller EF, Winding MHS, Stedmon CA.
545 2022. Vertical redistribution of principle water masses on the northeast Greenland Shelf. *Nature Communications* 13:
546 doi:10.1038/s41 467–022–35 413–z.

547 Hafrannsóknastofnun: Makrill *Scomber scombrus* Stofnmatskýrslur (stock assessment report), Hafrannsóknastofnun,
548 2024, https://www.hafogvatn.is/static/extras/images/mackerel_2024_techreport_is.html.

549 Hansen, B., and Østerhus, S.: North Atlantic–Nordic Seas exchanges, *Prog. Oceanogr.*, 45, 109–208, 2000.

550 Harden, B., Renfrew, I., and Petersen, G.: Meteorological buoy observations from the central Iceland Sea, *J. Geophys.*
551 *Res.-Atmos.*, 120, 3199–3208, 2015.

552 Harden, B. E., Pickart, R. S., Valdimarsson, H., Vage, K., de Steur, L., Richards, C., et al.: Upstream sources of the
553 Denmark Strait overflow: Observations from a high-resolution mooring array, *Deep-Sea Res. Pt. I*, 112, 94–112, 2016.

554 Hátún, H., and Chafik, L.: On the recent ambiguity of the North Atlantic Subpolar Gyre Index, *J. Geophys. Res.-Oceans*,
555 123, 5072–5076, 2018.

556 Hátún, H., Chafik, L., and Larsen, K. M. H.: The Norwegian Sea Gyre – a regulator of Iceland-Scotland Ridge exchanges,
557 *Front. Mar. Sci.*, 8, 1001, 2021.

558 Havik, L., Pickart, R. S., Våge, K., Torres, D. J., Thurnherr, A., Beszczynska-Möller, A., et al.: Evolution of the East
559 Greenland Current from Fram Strait to Denmark Strait: Synoptic measurements from summer 2012, *J. Geophys. Res.-*
560 *Oceans*, 122, 1974–1994, 2017.

561 Hersbach, H., Bell, B., Berrisford, P., et al.: The ERA5 global reanalysis, *Q. J. R. Meteorol. Soc.*, 146, 1999–2049,
562 <https://doi.org/10.1002/qj.3803>, 2020.

563 Holt, J., Schrum, C., Cannaby, H., Daewel, U., Allen, I., Artioli, Y., et al.: Potential impacts of climate change on the
564 primary production of regional seas: A comparative analysis of five European seas, *Prog. Oceanogr.*, 140, 91–115, 2016.

565 Holte, J., Talley, L. D., Gilson, J., and Roemmich, D.: An Argo mixed layer climatology and database, *Geophys. Res. Lett.*,
566 44, 5618–5626, 2017.

567 Huang J, Pickart RS, Chen Z, Huang RX. 2023. Role of air-sea heat flux on the transformation of Atlantic Water encircling
568 the Nordic Seas. *Nature Communications* 14: doi:10.1038/s41 467–023–35 889–3.

569 Ingvaldsen, R. B., Assmann, K. M., Primicerio, R., Fossheim, M., Polyakov, I. V., and Dolgov, A. V.: Physical
570 manifestations and ecological implications of Arctic Atlantification, *Nat. Rev. Earth Environ.*, 2, 874–889, 2021.

- 571 Jónsson, S.: The circulation in the northern part of the Denmark Strait and its variability, *ICES CM*, 50, 1999.
- 572 Jónsson, S., and Briem, J.: Flow of Atlantic water west of Iceland and onto the North Icelandic shelf, 2003.
- 573 Jónsson, S., and Valdimarsson, H.: Water mass transport variability to the North Icelandic shelf, 1994–2010, *ICES J. Mar.*
574 *Sci.*, 69, 809–815, <https://doi.org/10.1093/icesjms/fss024>, 2012.
- 575 Kohler, J., Serra, N., Bryan, F. O., Johnson, B. K., and Stammer, D.: Mechanisms of mixed-layer salinity seasonal
576 variability in the Indian Ocean, *J. Geophys. Res.-Oceans*, 123, 466–496, 2018.
- 577 Li, G., Cheng, L., Zhu, J., Trenberth, K. E., Mann, M. E., and Abraham, J. P.: Increasing ocean stratification over the past
578 half-century, *Nat. Clim. Chang.*, 10, 1116–1123, 2020.
- 579 Liu, C., Liang, X., Chambers, D. P., and Ponte, R. M.: Global patterns of spatial and temporal variability in salinity from
580 multiple gridded Argo products, *J. Clim.*, 33, 8751–8766, 2020.
- 581 Logemann, K., Ólafsson, J., Snorrason, A., Valdimarsson, H., and Marteinsdóttir, G.: The circulation of Icelandic waters
582 – a modelling study, *Ocean Sci.*, 9, 931–955, 2013.
- 583 Lozier, M. S., Li, F., Bacon, S., Bahr, F., Bower, A. S., Cunningham, S., et al.: A sea change in our view of overturning in
584 the subpolar North Atlantic, *Science*, 363, 516–521, 2019.
- 585 Macrander, A., Valdimarsson, H., and Jonsson, S.: Improved transport estimate of the East Icelandic Current 2002–2012,
586 *J. Geophys. Res.-Oceans*, 119, 3407–3424, 2014.
- 587 Mastropole, D., Pickart, R. S., Valdimarsson, H., Våge, K., Jochumsen, K., and Girton, J.: On the hydrography of Denmark
588 Strait, *J. Geophys. Res.-Oceans*, 122, 306–321, 2017.
- 589 Mauritzen, C.: Production of dense overflow waters feeding the North Atlantic across the Greenland-Scotland Ridge. Part
590 1: Evidence for a revised circulation scheme, *Deep-Sea Res. Pt. I*, 43, 769–806, 1996.
- 591 Moore, G. W. K., Våge, K., Pickart, R. S., & Renfrew, I. A. (2015). Decreasing intensity of open-ocean convection in the
592 Greenland and Iceland seas. *Nature Climate Change*, 5(9), 877–882.
- 593 Ólafsson, J.: Winter mixed layer nutrients in the Irminger and Iceland seas, *ICES Mar. Sci. Symp.*, 219, 329–332, 2003.
- 594 Intergovernmental Panel on Climate Change (IPCC): Special report on the ocean and cryosphere in a changing climate
595 (SROCC), 2019.
- 596 Ólafsdóttir, A. H., Utne, K. R., Jacobsen, J. A., Jansen, T., Óskarsson, G. J., Nøttestad, L., Elvarsson, B. Þ., Broms, C.,
597 and Slotte, A.: Geographical expansion of Northeast Atlantic mackerel (*Scomber scombrus*) in the Nordic Seas from 2007
598 to 2016 was primarily driven by stock size and constrained by low temperatures, *Deep-Sea Res. Pt. II*, 159, 152–168, 2019.
- 599 Østerhus, S., Woodgate, R., Valdimarsson, H., Turrell, B., De Steur, L., Quadfasel, D., Olsen, S. M., Moritz, M., Lee, C.
600 M., Larsen, K. M. H., and Jónsson, S.: Arctic Mediterranean exchanges: a consistent volume budget and trends in transports
601 from two decades of observations, *Ocean Sci.*, 15, 379–399, 2019.
- 602 Perez, F. F., Ólafsson, J., Olafsdóttir, S. R., Fontela, M., and Takahashi, T.: Contrasting drivers and trends of ocean
603 acidification in the subarctic Atlantic, *Sci. Rep.*, 11, 1–16, 2021.
- 604 Perez-Hernández, M. D., Pickart, R. S., Torres, D. J., Bahr, F., Sundfjord, A., Ingvaldsen, R., et al.: Structure, transport,
605 and seasonality of the Atlantic Water boundary current north of Svalbard: Results from a yearlong mooring array, *J.*
606 *Geophys. Res.-Oceans*, 124, 1679–1698, 2019.
- 607 Petit, T., Lozier, M. S., Josey, S. A., and Cunningham, S. A.: Atlantic deep water formation occurs primarily in the Iceland

608 Basin and Irminger Sea by local buoyancy forcing, *Geophys. Res. Lett.*, 47, e2020GL091028, 2020.

609 Petit, T., Lozier, M. S., Josey, S. A., and Cunningham, S. A.: Role of air-sea fluxes and ocean surface density on the
610 production of deep waters in the eastern subpolar gyre of the North Atlantic, *Ocean Sci. Discuss.*, 1–21, 2021.

611 Piron, A., Thierry, V., Mercier, H., and Caniaux, G.: Argo float observations of basin-scale deep convection in the Irminger
612 Sea during winter 2011–2012, *Deep-Sea Res. Pt. I*, 109, 76–90, 2016.

613 Polyakov, I. V., Pnyushkov, A. V., Alkire, M. B., Ashik, I. M., Baumann, T. M., Carmack, E. C., et al.: Greater role for
614 Atlantic inflows on sea-ice loss in the Eurasian Basin of the Arctic Ocean, *Science*, 356, 285–291, 2017.

615 Polyakov, I. V., Rippeth, T. P., Fer, I., Alkire, M. B., Baumann, T. M., Carmack, E. C., et al.: Weakening of cold halocline
616 layer exposes sea ice to oceanic heat in the eastern Arctic Ocean, *J. Clim.*, 33, 8107–8123, 2020.

617 Price, J. F., Weller, R. A., and Pinkel, R.: Diurnal cycling – Observations and models of the upper ocean response to diurnal
618 heating, cooling, and wind mixing, *J. Geophys. Res.-Oceans*, 91, 8411–8427, 1986.

619 Renfrew, I. A., Pickart, R. S., Våge, K., Moore, G. W., Bracegirdle, T. J., Elvidge, A. D., et al.: The Iceland Greenland
620 Seas Project, *Bull. Am. Meteorol. Soc.*, 100, 1795–1817, 2019.

621 Reynolds, R. and Banzon, V.: NOAA optimum interpolation 1/4 degree daily sea surface temperature (OISST) analysis,
622 version 2, NOAA Natl. Cent. Environ. Inf., 10, V5SQ8XB5, 2008.

623 Richardson, K. and Bendtsen, J.: Distinct seasonal primary production patterns in the sub-polar gyre and surrounding seas,
624 *Front. Mar. Sci.*, 2021.

625 Rudels, B., Björk, G., Nilsson, J., Winsor, P., Lake, I., and Nohr, C.: The interaction between waters from the Arctic Ocean
626 and the Nordic Seas north of Fram Strait and along the East Greenland Current: Results from the Arctic Ocean-02 Oden
627 expedition, *J. Mar. Syst.*, 55, 1–30, 2005.

628 Sallée, J.-B., Pellichero, V., Akhoudas, C., Pauthenet, E., Vignes, L., Schmidtke, S., et al.: Summertime increases in upper-
629 ocean stratification and mixed-layer depth, *Nature*, 591, 592–598, 2021.

630 Sarafanov, A.: On the effect of the North Atlantic Oscillation on temperature and salinity of the subpolar North Atlantic
631 intermediate and deep waters, *ICES J. Mar. Sci.*, 66, 1448–1454, 2009.

632 Sarmiento, J. L., Hughes, T. M., Stouffer, R. J., and Manabe, S.: Simulated response of the ocean carbon cycle to
633 anthropogenic climate warming, *Nature*, 393, 245–249, 1998.

634 Semper, S., Våge, K., Pickart, R. S., Valdimarsson, H., Torres, D. J., and Jónsson, S.: The emergence of the North Icelandic
635 Jet and its evolution from Northeast Iceland to Denmark Strait, *J. Phys. Oceanogr.*, 49, 2499–2521, 2019.

636 Shepherd, J. G., Brewer, P. G., Oschlies, A., and Watson, A. J.: Ocean ventilation and deoxygenation in a warming world:
637 Introduction and overview, 2017 [Dataset].

638 Skyllingstad, E. D., Samelson, R. M., Simmons, H., Laurent, L. S., Merrifield, S., Klenz, T., and Centurioni, L.: Boundary
639 layer energetics of rapid wind and wave forced mixing events, *J. Phys. Oceanogr.*, 53, 1887–1900, 2023.

640 Stewart, K. D. and Haine, T. W.: Thermobaricity in the transition zones between alpha and beta oceans, *J. Phys. Oceanogr.*,
641 46, 1805–1821, 2016.

642 Strehl, A.-M., Våge, K., Merdrud, S. L. H., and Barreyre, T.: A 70-year perspective on water-mass transformation in the
643 Greenland Sea: From thermobaric to thermal convection, *Prog. Oceanogr.*, 227, 103304, 2024.

644 Swift, J. H., Aagaard, K., and Malmberg, S.-A.: The contribution of the Denmark Strait overflow to the deep North Atlantic,

645 Deep-Sea Res. Pt. A, 27, 29–42, 1980.

646 Tesdal, J.-E., Abernathy, R. P., Goes, J. I., Gordon, A. L., and Haine, T. W.: Salinity trends within the upper layers of the
647 subpolar North Atlantic, *J. Clim.*, 31, 2675–2698, 2018.

648 Valdimarsson, H., Astthórsson, O. S., and Pálsson, J.: Hydrographic variability in Icelandic waters during recent decades
649 and related changes in distribution of some fish species, *ICES J. Mar. Sci.*, 69, 816–
650 825, <https://doi.org/10.1093/icesjms/fss027>, 2012.

651 Våge, K., Moore, G. W. K., Jónsson, S., and Valdimarsson, H.: Water mass transformation in the Iceland Sea, *Deep-Sea*
652 *Res. Pt. I*, 101, 98–109, 2015.

653 Våge, K., Papritz, L., Havik, L., Spall, M. A., and Moore, G. W. K.: Ocean convection linked to the recent ice edge retreat
654 along East Greenland, *Nat. Commun.*, 9, 1–8, 2018.

655 Våge, K., Pickart, R. S., Moore, G., and Ribergaard, M. H.: Winter mixed layer development in the central Irminger Sea:
656 The effect of strong, intermittent wind events, *J. Phys. Oceanogr.*, 38, 541–565, 2008.

657 Våge, K., Pickart, R. S., Spall, M. A., Moore, G., Valdimarsson, H., Torres, D. J., et al.: Revised circulation scheme north
658 of the Denmark Strait, *Deep-Sea Res. Pt. I*, 79, 20–39, 2013.

659 Våge, K., Pickart, R. S., Spall, M. A., Valdimarsson, H., Jónsson, S., Torres, D. J., et al.: Significant role of the North
660 Icelandic Jet in the formation of Denmark Strait Overflow Water, *Nat. Geosci.*, 4, 723–727, 2011.

661 Våge, K., Semper, S., Valdimarsson, H., Jónsson, S., Pickart, R. S., & Moore, G. W. K. (2022). Water mass transformation
662 in the Iceland Sea: Contrasting two winters separated by four decades. *Deep Sea Research Part I: Oceanographic Research*
663 *Papers*, 186, 103824.

664 Whitney, M. M. (2025). Icelandic riverine freshwater distribution, offshore export, and alongshelf connectivity. *Estuarine,*
665 *Coastal and Shelf Science*, 319, 109266.

666 Yamaguchi, R. and Suga, T.: Trend and variability in global upper-ocean stratification since the 1960s, *J. Geophys. Res.-*
667 *Oceans*, 124, 8933–8948, 2019.

668

669